Monthly Notices
of the
ROYAL ASTRONOMICAL SOCIETY

Mon. Not. R. Astron. Soc. **411,** 781–791 (2011) doi:10.1111/j.1365-2966.2010.17716.x

Lyman α wing absorption in cool white dwarf stars

R. D. Rohrmann,[1⋆] L. G. Althaus[2⋆†] and S. O. Kepler[3⋆]

[1] *Instituto de Ciencias Astronómicas, de la Tierra y del Espacio (CONICET), Av. España 1512 (sur), 5400 San Juan, Argentina*
[2] *Facultad de Ciencias Astronómicas y Geofísicas, UNLP, IALP-CCT (CONICET), Paseo del Bosque S/N, B1900FWA La Plata, Argentina*
[3] *Instituto de Física da UFRGS, 91501-900 Porto Alegre, RS-Brasil*

Accepted 2010 September 14. Received 2010 September 10; in original form 2010 June 10

ABSTRACT

Kowalski & Saumon identified the missing absorption mechanism in the observed spectra of cool white dwarf stars as the Lyman α red wing formed by the collisions between atomic and molecular hydrogen and successfully explained entire spectra of many cool DA-type white dwarfs. Owing to the important astrophysical implications of this issue, we present here an independent assessment of the process. For this purpose, we compute free–free quasi-molecular absorption in Lyman α due to collisions with H and H_2 within the one-perturber, quasi-static approximation. Line cross-sections are obtained using theoretical molecular potentials to describe the interaction between the radiating atom and the perturber. The variation in the electric dipole transition moment with the interparticle distance is also considered. Six and two allowed electric dipole transitions due to H–H and H–H_2 collisions, respectively, are taken into account. The new theoretical Lyman α line profiles are then incorporated in our stellar atmosphere program for the computation of synthetic spectra and colours of DA-type white dwarfs. Illustrative model atmospheres and spectral energy distributions are computed, which show that Lyman α broadening by atoms and molecules has a significant effect on the white dwarf atmosphere models. The inclusion of this collision-induced opacity significantly reddens spectral energy distributions and affects the broad-band colour indices for model atmospheres with $T_{\rm eff} < 5000$ K. These results confirm those previously obtained by Kowalski & Saumon. Our study points out the need for reliable evaluations of H_3 potential energy surfaces covering a large region of nuclear configurations, in order to obtain a better description of H–H_2 collisions and a more accurate evaluation of their influence on the spectrum of cool white dwarfs.

Key words: atomic processes – line: profiles – molecular processes – stars: atmospheres – white dwarfs.

1 INTRODUCTION

White dwarf (WD) stars represent the most common final stage of the stellar evolution and as such convey valuable information about the history of our Galaxy and stellar populations (see Althaus et al. 2010 for a recent review). The large majority of observed WDs show hydrogen-rich atmospheres (DA WDs). Since the spectrum of light escaping from old and cool WDs controls the rate at which they cool, the evaluation of cooling time-scales of such WDs is sensitive to the gas/fluid opacity and equations of state used in the model atmospheres (Hansen 1998; Salaris et al. 2000; Serenelli et al. 2001). Furthermore, model atmospheres are a basic tool in the analysis of observed spectroscopy and photometric data. In this sense, the computation of synthetic spectra helps to reveal important details about the physical processes in the external layer of WDs and to understand the spectral evolution of these objects.

Photometric observations presented and analysed by Bergeron, Leggett & Ruiz (1997) for 110 cool WDs showed a flux deficiency in the B magnitude for stars cooler than $T_{\rm eff} \approx 5500$ K. The ultraviolet (UV) absorption there was interpreted to be a missing opacity source due to hydrogen. By computing the Lyman α quasi-molecular absorption and successful fits to the entire spectra of cool hydrogen atmosphere WDs, Kowalski & Saumon (2006) (hereinafter KS) identified the origin of B deficiency as the Lyman α line broadened by collision of absorbing H atom with H_2 molecules.

Quasi-molecular radiative transitions occur when a photon is absorbed or emitted by a hydrogen atom while it interacts with one or more neighbouring particles (atom, ion or molecule) at atom–perturber separations of few Å. The interaction between the absorber atom and other particles at short distances eventually leads

⋆E-mail: rohr@icate-conicet.gob.ar (RDR); althaus@fcaglp.unlp.edu.ar (LGA); kepler@if.ufrgs.br (SOK)
†Member of the Carrera del Investigador Científico y Tecnológico, CONICET, Argentina.

to the formation of well-known molecular satellites in the line wings (Sando & Wormhoudt 1973; Stewart, Peek & Cooper 1973; Allard & Kielkopf 1982). Lyman α satellites have been observed in the spectra of DA WDs and identified as produced by $H + H^+$ (1405-Å satellite) and H + H (1623-Å satellite) collisions by Nelan & Wegner (1985) and Koester et al. (1985), respectively. A broad H_2 collision induced satellite in the red wing of Lyman β at 1150 Å has also been detected by Allard et al. (2004) in the bright pulsating DA WD G226−29.

Classical resonance and van der Waals broadening have been demonstrated to be inadequate (Sando, Doyle & Dalgarno 1969) in reproducing the Lyman α red wing extending far into the optical region. These broadening evaluations assume that the interaction between the radiating atom and perturber follows a power-law dependence r^{-p} with the interparticle distance r (e.g. $p = 3$ for resonance broadening and $p = 6$ for van der Waals broadening, cf. Mihalas 1978), which fails to describe true interatomic potentials at r smaller than few Å where far-wing contributions are produced. Appropriate wing absorption theories are based on quasi-molecular approaches, which use accurate theoretical molecular potentials to describe the interaction between the radiator and perturber and take into account the variation in electric dipole transition moment with the interparticle distance (e.g. Jablonski 1945; Bates 1951; Chen & Takeo 1957; Gallager & Holstein 1977; Allard & Kielkopf 1982). More specifically, the spectrum of absorption is evaluated using *ab initio* calculations of Born–Oppenheimer energies and dipole transition moments for the electronic states of the quasi-molecule or dimer formed during the collision.

Atmosphere model evaluations for cool WDs that included Lyman α line broadening based on quasi-molecule methods were performed by Koester & Wolff (2000), Wolff, Koester & Liebert (2002) and KS. KS were successful in reproducing the spectrum of cool DA WDs due to the inclusion of broadening by H–H_2. Koester & Wolff (2000) used only broadening by H–H and H–He collisions. KS evaluations were based on the semiclassical approximation, which is generally considered valid to describe the far wings of the line profile. This approach takes into account the variation in the dipole moment during an atomic collision. Koester & Wolff's (2000) calculations have been made using the quasi-static limit of the so-called unified theory (Allard et al. 1999). In the formalism of the unified theory, the whole line profile from the line core to the far wings can be assessed. It also takes into account additional contributions from multiple perturber collisions,[1] which are considered important at perturber densities larger than 10^{21} particles per cm^3. The so-called static limit of the unified description produces a line spectrum similar to that of the semiclassical approximation.

Given that more than 80 per cent of the WD population is of DA type (Eisenstein et al. 2006; Althaus et al. 2010), Lyman α wing broadening could have implications on the luminosity function of very old WDs. It is thus of much interest to study the wings of the Lyman α absorption line yielded in atomic collisions. Considering KS opacity calculations showed that the Lyman α quasi-molecular opacity may have an important role in affecting the emergent UV and blue radiation of cool DA WD stars, we have performed an independent evaluation. KS showed only results based on their estimation of the main contributions to the gas opacity from H–H and H–H_2 encounters. Here, we present results including all dipole-allowed transitions resulting from these collisions and show an overall analysis of the relative importance among them. For computing Lyman α wing opacity, we have selected the semiclassical broadening theory as a matter of convenience at the present stage of our calculations to reproduce KS calculation conditions and for comparison purposes in future works. We postpone to develop wing broadening evaluations based on the unified method to a later work. As this paper is devoted to cool DA-type WDs, we only include collisions of radiating H atoms with atoms and molecules.

This paper is structured as follows. In Section 2, we briefly review the semiclassical broadening method and assess at some length the wing broadening arising from collisions of H atoms and H_2 molecules. The line opacity including non-ideal gas effects on the upper state of transitions is shown in Section 2.4. Model atmospheres and input physics are detailed in Section 3. We then evaluate in Section 4 the implications of our line-broadening opacity on the emergent spectrum of cool WDs. Finally, in Section 5, we summarize the main conclusions.

2 LINE-BROADENING THEORY

In the electric dipole approximation, the cross-section σ_ν of the radiation absorption corresponding to a transition from an initial state i to a final state j of an atom or molecule is given by

$$\sigma_{ij}(\nu) = 4\pi^2\alpha\nu|T_{ij}|^2\phi_{ij}(\nu), \tag{1}$$

where α is the fine-structure constant, ν is the frequency of the transition, T_{ij} is the electric dipole transition moment and $\phi_{ij}(\nu)$ is the normalized line profile

$$\int_0^\infty \phi_{ij}(\nu)\mathrm{d}\nu = 1. \tag{2}$$

For radiation unpolarized and randomly oriented particles $|T_{ij}|^2 = \frac{1}{3}D_{ij}(r)$, with $D_{ij}(r)$ the so-called dipole strength function for the transition $i \rightarrow j$. As a reference, the Lyman α transition (i = 1s, j = 2p) of isolated hydrogen atoms (Bethe & Salpeter 1957) has a central frequency $\nu_0 = 2.467 \times 10^{15}$ Hz, $D_{1s,2p} = (32/27)^3 a_0^2$ (a_0 is the Bohr radius) and the resulting total cross-section is

$$\int_0^\infty \sigma_{1s,2p}(\nu)\mathrm{d}\nu = \frac{4\pi^2\alpha}{3}\nu_0 D_{1s,2p} = 1.1044 \times 10^{-2}\,\mathrm{cm}^2. \tag{3}$$

2.1 The quasi-static approach

Our calculation of the wing absorption of Lyman α is made within the semiclassical approximation following the methodology used in KS. This approach is based on the following assumptions:

(i) *Born–Oppenheimer approximation*: nuclei move on single adiabatic potential energy surfaces (PESs) created by the much faster moving electrons.

(ii) *Adiabatic collisions*: the interaction between two particles is viewed as the formation of a quasi-molecule which moves over a particular Born–Oppenheimer energy curve during the collision.

(iii) *Nearest neighbour approximation*: the radiating atom is assumed to be only perturbed by its nearest neighbour.

(iv) (*Classical*) *Franck–Condon principle*: the radiative transition occurs in the neighbourhood of the internuclear distance, where the difference between upper and lower potentials of the quasi-molecule equals the photon energy.

[1] It is not clear, however, how the simultaneous perturbation of various *different* type of particles could be considered by this method.

The first enumerated approximation is used to identify collisionally perturbed atomic states as parts of the initial and final molecular adiabatic states. The second assumption is considered valid in slow atomic collisions (Hirschfelder, Curtiss & Bird 1954) and seems appropriate for the temperatures of cool WD atmospheres.[2] In the one-perturber approach, we ignore multiple simultaneous encounters. Classically, the fourth assumption considers that the radiative decay time is short compared to the collision time.

Within the preceding assumptions, the quasi-static approximation predicts the following expression of the line profile (Margeneau & Lewis 1959; Allard & Kielkopf 1982):

$$\phi_{ij}(\nu) = \frac{h}{|\mathrm{d}V_{ij}/\mathrm{d}r|} P_1(r), \tag{4}$$

where, h is the Planck constant and $V_{ij}(r)$ is the difference between the two Born–Oppenheimer energies $V_j(r)$ and $V_i(r)$ representing the interaction of the active atom, in each one of two states i and j involved in the transition, with a perturber at a distance r. The first factor of the right-hand side in equation (4) takes into account the relationship between the atom–perturber distance and transition frequency ν, which is given by

$$h\nu = V_{ij}(r) \equiv V_j(r) - V_i(r). \tag{5}$$

The function $P_1(r)$ in equation (4) is the probability density of finding the nearest perturber to a distance r from the radiator:

$$P_1(r) = 4\pi n_\mathrm{p} r^2 \exp\left(-4\pi n_\mathrm{p} r^3/3\right), \tag{6}$$

where n_p being the mean density of perturbers in the gas. The exponential factor in equation (6) is usually negligible numerically and is often omitted; however, it is necessary to obtain the correct normalization of the profile $\phi_{ij}(\nu)$ (equation 2).

With equation (4), the cross-section in equation (1) may be written as

$$\sigma_{ij}(\nu) = \frac{4\pi^2\alpha}{3} \frac{h\nu}{|\mathrm{d}V_{ij}/\mathrm{d}r|} D_{ij}(r) P_1(r) \mathrm{e}^{-\beta V_i(r)}, \tag{7}$$

where $\beta = (kT)^{-1}$, k is the Boltzmann constant and T is the gas temperature. The exponential factor in equation (7) is introduced as part of the Boltzmann distribution function of H atoms and accounts for the probability of finding perturbed atoms in the lower state i with respect to unperturbed atoms [$V_i(r \to \infty) = 0$]. If the potential difference $V_{ij}(r)$ has an irregular behaviour and there are several distances r verifying the relationship (5), we have to sum over all atom–perturber configurations that contribute to the wing broadening at the frequency ν.

The total cross-section of a specific collision-induced absorption (CIA) line is a sum over all lower (i) and upper (j) molecular states, which can contribute to the wing broadening. These contributions are additive in the Born–Oppenheimer approximation with appropriate statistical weights π_{ij}. In particular, there are many contributions to the resonance broadening of the Lyman α line corresponding to transitions of different quasi-molecular aggregates. In cool DA WDs, the main perturbers are H atoms and H_2 molecules, because they are the most-abundant species. In the following sections, we consider wing broadening arising from collisions of H atoms with these particles.

[2] This approximation breaks down for high-energy collisions, which can result in either ionization or excitation to other electronic states. Such collisions constitute non-adiabatic processes and are considered negligible in this work.

Table 1. H_2 states asymptotically correlated with H(1s) + H(1s, 2s, 2p).

State	T_e (cm^{-1})	g_e	Dissociation product	Energy curve
$X^1\Sigma_g^+$	0	1	H(1s) + H(1s)	[a]
$b^3\Sigma_u^+$	36 113[b]	3	H(1s) + H(1s)	[c]
$B^1\Sigma_u^+$	90 203	1	H(1s) + H(2p)	[d]
$c^3\Pi_u^+$	95 091	6	H(1s) + H(2p)	–
$a^3\Sigma_g^+$	95 226	3	H(1s) + H(2p)	[c]
$C^1\Pi_u^+$	99 150	2	H(1s) + H(2p)	[a]
$E^1\Sigma_g^+$	99 164	1	H(1s) + H(2s)	–
$e^3\Sigma_u^+$	106 832	3	H(1s) + H(2s)	–
$B'^1\Sigma_u^+$	110 478	1	H(1s) + H(2s)	[d]
$f^3\Sigma_u^+$	111 752	3	H(1s) + H(2p)	–
$G^1\Sigma_g^+$	111 812	1	H(1s) + H(2p)	–
$h^3\Sigma_g^+$	112 021	3	H(1s) + H(2s)	[c]
$I^1\Pi_g^+$	112 072	2	H(1s) + H(2p)	–
$i^3\Pi_g^+$	112 216	6	H(1s) + H(2p)	[c]

[a] Kolos & Wolniewicz (1965).
[b] Unbound state.
[c] Staszewska & Wolniewicz (1999).
[d] Wolniewicz & Dressler (1988).

2.2 H–H collisions

Table 1 lists the products of H(1s)–H(1s, 2s, 2p) adiabatic collisions, including the equilibrium electronic energy T_e for ground rotovibrational levels as given by Field, Sommerville & Dressler (1966), the multiplicity g_e of each state and the data source for energy curves relevant to this work.

According to the adiabatic approximation, from the encounter of two H atoms, one in the state 1s and the other in the state 2p, one of eight possible H_2 electronic states is formed (Table 1). However, only four ($B^1\Sigma_u$, $a^3\Sigma_g$, $C^1\Pi_u$ and $i^3\Pi_g$) of these molecular levels have allowed electric dipole transitions with the lowest H_2 states, $X^1\Sigma_g^+$ and $b^3\Sigma_u^+$, which asymptotically correlate with two separated H(1s) atoms. Similarly, there are four H_2 levels, which can be formed from adiabatic collisions of H(1s) and H(2s) atoms (Table 1), but only two ($B'^1\Sigma_u$ and $h^3\Sigma_g$) of these states have allowed dipolar transitions to states $X^1\Sigma_g^+$ and $b^3\Sigma_u^+$. Only states involved in molecular transitions allowed by electronic selection rules are of interest in this study.

The complete set of electric dipole radiative processes contributing to the Lyman α wing from H–H collisions is illustrated in Fig. 1. The conditional probability $P(i|i \to j)$, with values shown in Fig. 1, is the probability that a quasi-molecule in the state i is formed from a specific H(1s)–H(1s,2s or 2p) collision, under the condition that $i \to j$ is an allowed electric dipole transition contributing to the Lyman α wing (similar definition follows for $P(j|j \to i)$). The classical evaluation of $P(i|i \to j)$ takes into account that if two particles approach adiabatically each other, the fraction of occasions on which they move along a particular energy curve (say i) is given by the ratio of the statistical weight of this curve (g_i) to the sum of the statistical weights of all possible curves.

The Born–Oppenheimer energy curves arising from H–H collisions that contribute to the Lyman α wings are shown in Fig. 2. The potential curves adopted in this work are referenced in Table 1. As the atom and perturber get farther away from each other, the electronic energies tend to asymptotic values, which are sums of individual particle energies. Since atomic states are degenerate, there are in general several molecular energy curves that tend to the same asymptotic energy.

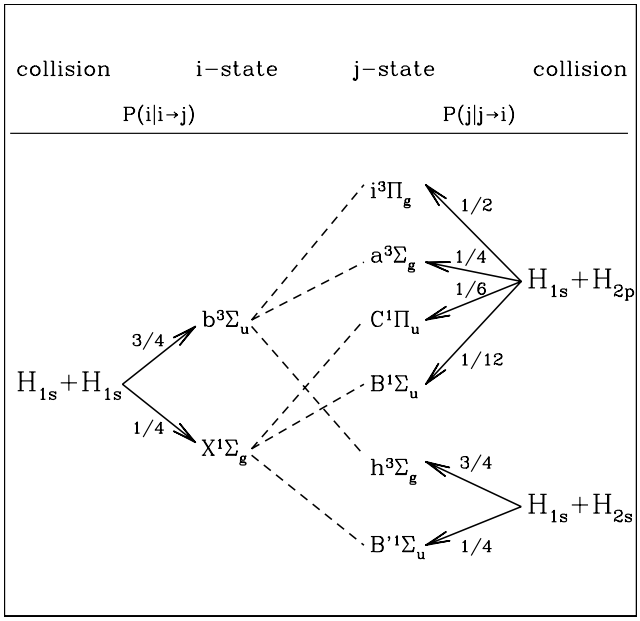

Figure 1. Collision diagram for H(1s) + H(1s, 2s, 2p) encounters with intermediate quasi-molecular states connected by allowed electric dipole transitions (dashed lines). Conditional probabilities of electronic state formation (see text) are indicated on the plot.

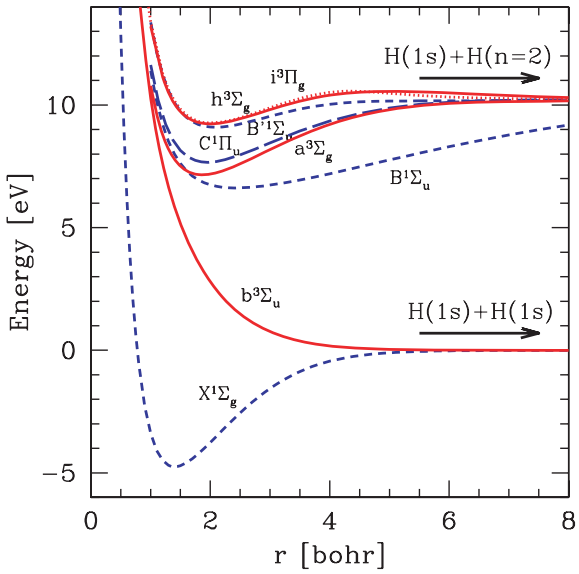

Figure 2. Born–Oppenheimer energies of H_2 states relevant to this paper. Dashed lines are for singlet Σ states, solid lines for triplet Σ states, long-dashed line for the $C^1\Pi_u^+$ state and the dotted line for the $i^3\Pi_g^+$ state. The asymptotic states corresponding to great internuclear separations are also indicated.

The dipole moments of molecular transitions allowed by electronic selection rules are shown in Fig. 3. The dipole forbidden character of the transition (1s to 2s) for separated atoms is associated to electric dipole transition moments of the H_2 molecule, $T_{X-B'}$ and T_{b-h}, which become zero as the internuclear separations $r \to \infty$. On the other hand, the correct dipole transition moment for the 1s to 2p atomic transition is obtained in the dissociation limit for $X - B$, $X - C$, $a - b$ and $h - b$ transitions.

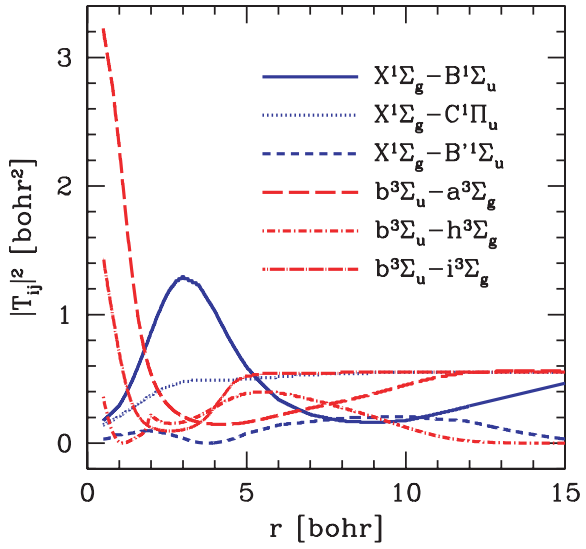

Figure 3. $|T_{ij}|^2$ dipole moments between H_2 states, which correlate with H(2s or 2p) + H(1s) and H(1s) + H(1s) as a function of the internuclear distance. Data taken from Dressler & Wolniewicz (1985) for $X - B$ and $X - C$, from Ford et al. (1975) for $X - B'$, and from Staszewska & Wolniewicz (1999) for triplet state transitions.

To obtain the total absorption coefficient $\sigma_{H-H}(\nu)$ due to H–H encounters, a sum of (7) over all H_2 transitions, which contribute at the frequency ν, must be performed:

$$\sigma_{H-H}(\nu) = \sum_{ij} \pi_{ij}\sigma_{ij}(\nu). \quad (8)$$

In the present case, the weights π_{ij} of these contributions are directly related to the probabilities $P(j|j \to i)$. It can be demonstrated that (8) recovers the correct limit value for asymptotically separated atoms as given by (3).

2.3 H–H_2 collisions

Adiabatic collisions between H atoms and H_2 molecules form triatomic systems. The analysis for atom–atom collisions in Section 2.2 was simplified by the fact that only a single internuclear coordinate, the atom–atom distance r, need be considered. In the present case, however, collision processes involving H_2 molecule and H atoms are functions of the interparticle distance r and also of the molecular orientation, which can be characterized by a single angle θ in the case of a homopolar diatomic molecule [θ is the angle defined between the line connecting the H atom to the bisector of the molecular axis; see geometrical configuration in Fig. 5 (inset) shown later]. Consequently, the Bohr–Oppenheimer energy solutions for the polyatomic molecule H_3 consist of energy surfaces instead of energy curves.

Following Peng, Kristyan & Kuppermann (1995), we denote by E_1, E_2, E_3 and E_4 the four lowest PESs of the H_3 system. E_1 labels the ground electronic state, which asymptotically separates into $H_2(X^1\Sigma_g)$+H(1s). The first excited state of H_3, E_2, adiabatically dissociates into $H_2(b^3\Sigma_u)$+H(1s) and undergoes a conical intersection with the ground state at equilateral triangle (D_{3h}) geometries. E_1 and E_2 become the degenerate $2p^2E'$ state at D_{3h} structures and constitute a well-known Jahn–Teller system. The next two excited states, E_3 and E_4 ($2s^2A_1'$ and $2p^2A_2''$ states in D_{3h} symmetry), correlate with $H_2(X^1\Sigma_g)$+H(2s) and $H_2(X^1\Sigma_g)$+H(2p), respectively.

These states are the lowest Rydberg states of H_3 and are located very close in energy for all geometries.

It must be noted that the (E_2) low-lying excited state is not relevant to this study, because it correlates with the $b^3\Sigma_u$ *unbound* electronic state of the H_2 molecule rather than excited states of the H atom.[3] Therefore, the polyatomic states of interest here are E_1, E_3 and E_4. These H_3 states are sufficient to infer the likely course of an encounter between H and H_2 contributing to the Lyman α wing absorption (Mayne et al. 1984, hereinafter Ma).

The evaluation of PESs is computationally expensive compared with similar studies of diatomic molecules. Theoretical calculations are often depending on the quantum chemical method applied and, in general, it is not easy to identify the best available PES, especially for excited electronic states. Moreover, in the case of triatomic hydrogen, excited-state energies are often available for a few nuclear configurations so that interpolations or fit procedures are required to cover a large region of the nuclear geometry as it is necessary in the analysis of H–H_2 collisions. Accurate energy data obtained by Liu (1973) and Siegbahn & Liu (1978) for the H_3 ground state have been fitted by Truhlar & Horowitz (1978, 1979) (hereinafter TH). This fit is considered one of the four most accurate and widely used PESs for the H_3 system (Mielke, Garret & Peterson 2002). Unfortunately, energy data of the first Rydberg states are limited to a few geometries. Kulander & Guest (1979) (hereinafter KG) carried out calculations along an equilateral insertion path ($\theta = 90^\circ$). Roach & Kuntz (1986, hereinafter RK) used the diatomic-in-molecules (DIM) procedure to calculate the ground and lower lying excited PESs over several geometries, particularly for a 45° angle of approach. Energy computations of Petsalakis, Theodorakopoulos & Wright (1988) were performed mainly for the collinear H+H_2 approach ($\theta = 0^\circ$) and linear symmetric H_3, and for a few perpendicular trajectories. More recent evaluations of Rydberg energies due to Peng et al. (1995) also contain few data points. A semi-empirical PES of the first H_3 Rydberg states was developed by Ma based on evaluations in the DIM approximation (Raynor & Herschbach 1982).

Some of these energy evaluations are shown in Fig. 4 for non-collinear configurations, $\theta = 90^\circ$ being the more probable condition of impact. TH analytical representation for the ground state agrees remarkably well with DIM evaluations of RK at $\theta = 45^\circ$ and with theoretical calculations of KG at $\theta = 90^\circ$. The equilibrium internuclear separation of the H_2 molecule was fixed at $R = 1.4$ Bohr (0.74 Å), except in the case of KG evaluations, which are based on the equilibrium distance of the H_3^+ molecule ($R = 1.65$ Bohr, this is only slightly larger than the bond length of 1.62 Bohr for H_3). Fig. 4 also shows values of the analytic fit due to Ma for the first Rydberg states at $\theta = 90^\circ$ (equivalent energy is assumed for E_3 and E_4 in this work). Ma fit yields smaller values than those from KG calculations throughout the region $2 < r < 4.5$. At H–H_2 separations ≈2 Bohr, the Ma curve crosses the KG curve and remains above that for shorter distances.

For comparison, we have also plotted in Fig. 4 the results used by KS, based on theoretical studies of Boothroyd et al. (1991, 1996). We have not incorporated results of Boothroyd et al. in our wing opacity evaluations, because no information is available to which asymptotic state the evaluated levels correlate with, and there are not enough analysed geometrical configurations to correctly identify the E_3 and E_4 states from the computed data points (Boothroyd, private communication). The ground energy curve used by KS at $\theta = 90^\circ$

[3] The E_2 state could be involved in ternary collisions, since it asymptotically correlates with 3H(1s).

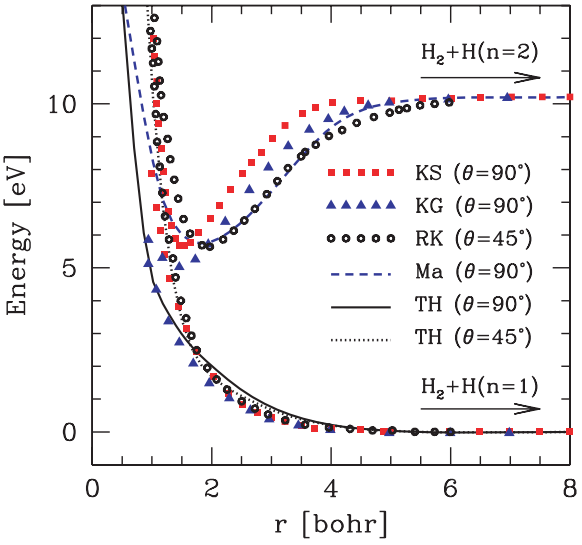

Figure 4. Electronic states of H_3, which in the asymptotic region H+H_2 correlate with H(2s or 2p) + $H_2(X^1\Sigma_g^+)$ and H(1s) + $H_2(X^1\Sigma_g^+)$ as a function of the H–H_2 interparticle distance r and for collision angles θ = 45° and 90°. Data taken from KS: Kowalski & Saumon (2006) (fig. 1), KG: Kulander & Guest (1979) (fig. 1), Roach & Kuntz (1986) (fig. 5), Ma: Mayne et al. (1984) (analytic fit) and TH: Truhlar & Horowitz (1978, 1979) (analytic fit).

lies above the TH and KG evaluations at H–H_2 separations smaller than 1.7 Bohr. For the first Rydberg state, KS results remain above those of KG at distances smaller than about 5 Bohr with deviations of ≈0.8 eV for intermediate distances up to 1.5 Bohr and increasing differences at smaller distances.

From this limited amount of PESs, one is already able to see the complexity in the selection of appropriate PESs to be used in opacity evaluations. Three important facts deserve to be mentioned: (i) $r < 2$ Bohr represents the critical region where absorptions to optical spectrum could be yielded, (ii) energy differences between E_1, E_2 and E_3 states play a decisive role in defining this spectrum, and (iii) among the available PES data, KG and RK results provide simultaneous and self-consistent evaluations of energies for these states. Hence, we decided to adopt KG and RK data to develop PESs for the ground and lowest Rydberg states. In practice, we have considered the E_3 and E_4 potential energies identical because they are similar for all molecular geometries (differences smaller than 1000 cm^{-1}, Ma) and because they cannot be clearly distinguished from one another in the available data. In order to construct PESs covering a large range of nuclear geometries, we use angular interpolation between KG ($\theta = 90^\circ$) and RK ($\theta = 45^\circ$) evaluations. In this sense, it is worth noting that the largest contribution to the absorption cross-section comes from perpendicular collision paths [the averaged-angle cross-section, see equation (9) later in this section, concentrates the integration weight near the configuration $\theta = 90^\circ$]. To complete the PESs, we maintained the RK values for $\theta < 45^\circ$. We have verified that this choice introduces a minor uncertainty in the cross-section computation. The consequences for the wing absorption calculation due to the adopted PESs and the use of alternative PESs based on TH and Ma fits will be discussed in Section 4.

Although the energy surfaces for the E_3 and E_4 excited electronic states are nearly identical, the electric dipole moment between these states and the ground state differs significantly. In this study, we adopt dipole moment transitions based on evaluations of

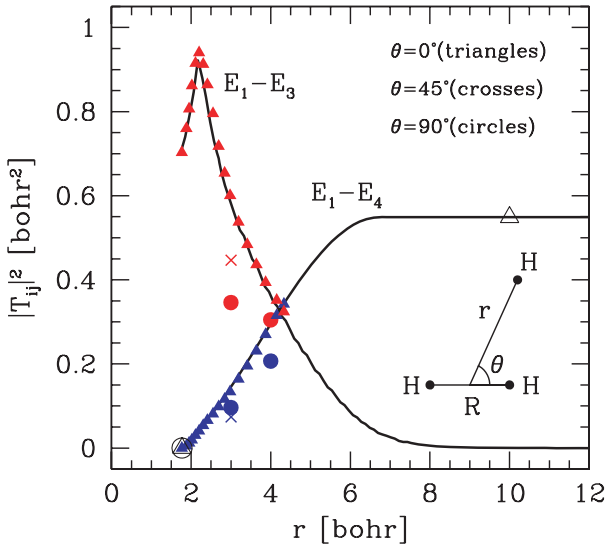

Figure 5. $|T_{ij}|$ dipole moments of E_1 to E_3 and E_1 to E_4 polyatomic transitions as a function of the nuclear geometry. Data taken from Petsalakis et al. (1988) and Peng et al. (1995) are represented with the fill and open symbols, respectively. Lines indicate our fits to results of Petsalakis et al. and Peng et al. for $\theta = 0°$.

Petsalakis et al. (1988) and Peng et al. (1995). Analytical fits including internuclear distances and collision angles beyond the data range were used in our calculations. Fig. 5 shows that the $|T_{ij}|$ transition moment between the E_1 and E_4 states increases with the atom–diatomic distance from $r \approx 1.8$ Bohr and approaches its theoretical value of 0.74 Bohr when $r \to \infty$. In D_{3h} symmetry configuration, this transition is forbidden. At short interparticle distances ($r < 4$ Bohr), the transition from the ground state to the E_3 state is predicted to be considerably stronger than the transition to the E_4 state. Although the E_1–E_3 transition is allowed, it decreases above $r \approx 2$ Bohr and approaches zero for $r \to \infty$, in agreement with that expected in the dissociation limit where the 1s → 2s atomic transition is forbidden.

Finally, the total cross-section for Lyman α wing broadening by H–H_2 collisions is averaged over all collision-frame angles and expressed as

$$\sigma_{\mathrm{H-H_2}}(\nu) = \sum_{ij} \frac{\pi_{ij}}{2} \int_0^{\pi} \sigma_{ij}(\nu, \theta) \sin\theta \, \mathrm{d}\theta \qquad (9)$$

where the summation comprises $E_1 \to E_3$ and $E_1 \to E_4$ transitions and $\sigma_{ij}(\nu, \theta)$ is given by equation (7) with $V_{ij}(r, \theta)$, $D_{ij}(r, \theta)$ and $V_i(r, \theta)$ functions of both the distance r and angle orientation θ of the dimer. The π_{ij} weights were chosen so that, using the asymptotic values of H_3 transition moment, the isolate atom limit is recovered (equation 3).

2.4 Total collision-induced wing absorption

The lines profiles $\sigma_{\mathrm{H-H}}(\nu)$ and $\sigma_{\mathrm{H-H_2}}(\nu)$ given by equations (8) and (9) have been convolved with a Doppler profile to take into account the thermal broadening introduced by the particle motions. We have prepared detailed opacity tabulations of these cross-sections appropriate for atmosphere model calculations. These results are available in the website http://www.fcaglp.unlp.edu.ar/evolgroup.

The total Lyman α wing profile $\sigma_{\mathrm{tot}}(\nu)$ is sensitive to the relative abundance of the different perturbers responsible for the line broadening. Within the nearest neighbour quasi-static approach, the relative contributions to the line broadening by H and H_2 are given by the probabilities of finding an atom or molecule as the closest neighbour of radiating atoms. These probabilities can be approximated by the molar fractions of atoms (x_{H}) and molecule ($x_{\mathrm{H_2}}$) (e.g. Rohrmann & Zorec 2006), resulting in

$$\sigma_{\mathrm{tot}}(\nu) = x_{\mathrm{H}} \sigma_{\mathrm{H-H}}(\nu) + x_{\mathrm{H_2}} \sigma_{\mathrm{H-H_2}}(\nu). \qquad (10)$$

Finally, the extinction coefficient (units of cm^{-1}) due to CIAs in the Lyman α line is

$$\chi(\nu) = n_{\mathrm{H}(n=1)} \sigma_{\mathrm{tot}}(\nu), \qquad (11)$$

where $n_{\mathrm{H}(n=1)}$ is the number density (in cm^{-3}) of atoms in the ground state.

3 MODEL ATMOSPHERES

The local thermodynamic equilibrium model atmosphere code used in our analysis is a modified version of that described at length in Rohrmann (2001) and Rohrmann et al. (2002), which is appropriate for hydrogen and helium atmospheric compositions (including mixed and pure models). Models are computed assuming hydrostatic and radiative–convective equilibrium. Energy transport by convection present in the cool atmospheres considered here is treated within the usual mixing length theory, where we have assumed the so-called ML2 parametrization of the convective flux.

The gas model used in the code includes the species H, H_2, H^+, H^-, H_2^+, H_3^+, He, He^-, He^+, He^{2+}, He_2^+, HeH and free electrons. The relative abundances of these species is determined by the occupation probability formalism (Hummer & Mihalas 1988) (hereinafter HM). The calculated level occupation probabilities are then explicitly included in the calculation of the line and continuum opacities as described in Section 3.1.

The Lyman α wing opacity analysed in the preceding sections represents a partial contribution to the total gas opacity in atmospheres of cool DA WDs. For pure hydrogen models, the opacity sources in the numerical code also include bound–free (H, H^-, H_2^+) and free–free (H, H_2, H_3, H^-, H_2^-, H_2^+) transitions, electronic and Rayleigh (H, H_2) scattering, CIAs of H–H (Doyle 1968), H–H_2 (Gustafsson & Frommhold 2003) and H_2–H_2 (Borysow, Jorgensen & Fu 2001), and the most significant H line series. Details are described at length in Rohrmann et al. (2002). It should be pointed out that the H_2–H_2 CIA consists of rotovibrational transitions of H_2 induced by molecular collisions, which has a strong influence on the infrared spectrum of cool WDs.

3.1 Non-ideal effects in opacity laws

One important advancement in WD atmosphere modelling has been made by the use of the occupation probability formalism of HM. The HM approach considers the perturbations on each atom or molecule by charged and neutral particles and includes their effects in the evaluation of atomic populations and equations of state of the gas. The interactions with neutral particles are treated within the hard sphere model and those with charged particles are calculated with microfield distribution functions. The internal partition function of a given species can then be written as

$$Z = \sum_i w_i g_i \, \mathrm{e}^{-\beta E i} \qquad (12)$$

where E_i and g_i are, respectively, the excitation energy and multiplicity of the level i. The function w_i, the so-called probability

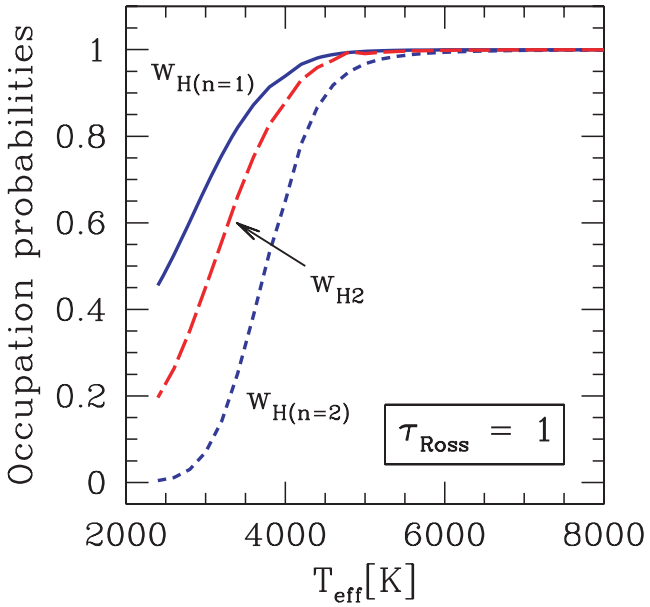

Figure 6. Occupation probabilities of the $n = 1$ (dotted line) and $n = 2$ (dashed line) hydrogen states and of the ground H_2 molecule state (long-dashed line) calculated in the photosphere ($\tau_{\rm Ross} = 1$) of $\log g = 8$, hydrogen pure models as a function of the effective temperature.

occupation of the level, is computed self-consistently with the non-ideal term in the gas free-energy. The values of w_i decrease continuously and monotonically as the strength of the relevant interaction increases and avoid the familiar divergence of internal partition functions. Analytical continuity of all thermodynamical properties of the gas is assured by the application of the free-energy minimization technique. Details of HM evaluations are given in Rohrmann et al. (2002). Fig. 6 shows the occupation probabilities of the lowest bound states of H and H_2 at a Rosseland mean optical depth $\tau_{\rm Ross} = 1$ for model atmospheres at $2400 < T_{\rm eff} < 8000$ K and $\log g = 8$. Considering that the dominant perturbers in atmospheres of cool WDs are neutral particles, the occupation probabilities are mainly determined by the hard sphere model. The transition of w_i from near-unity to near-zero is a monotonically decreasing function of the gas density which, in Fig. 6, increases with decreasing $T_{\rm eff}$.

Because the pressure shifts observed experimentally for hydrogen lines are very small (Wiese, Kelleher & Paquette 1972) and there is lack of a reliable theory to compute energy level shifts in bound particle states, the HM formalism uses energy eigenvalues of isolated particles. Non-ideal effects are therefore directly accounted for in w_i factors leading to the concept of an effective statistical weight for bound states, whereas the internal particle structure is assumed unperturbed. This includes the use of oscillator strengths of isolated atoms. However, since the relative population between two particle levels is modified with respect to ideal (Boltzmann or Saha) relations (as it can be inferred from equation 12), the atomic transition rates must be accordingly adapted to satisfy the principle of detailed balancing at thermodynamic equilibrium. If we denote the transition probability per second from i to j levels of an unperturbed atom by Λ_{ij}, then the transition rate $i \rightarrow j$ for a non-ideal gas in the HM approach is given by (Hubeny, Hummer & Lanz 1994; Rohrmann et al. 2002):[4]

$$n_i \Lambda_{ij} w_j. \tag{13}$$

This phenomenological proposal preserves the well-known Einstein and Einstein–Milne relations on the Λ_{ij} coefficients. Thus, $\Lambda_{ij} w_j$ plays the role of a conditional probability, such that it approaches to Λ_{ij} (the value corresponding to isolated particles) for non-perturbed transition final states and approaches to zero for strongly perturbed levels. Expression (13) is applied to all bound–bound and bound–free transitions with the convention that bare ions formally have $w_j = 1$.

The evaluation of the Lyman α wing opacity (and CIA processes in general) departs from the non-ideal opacity laws of the HM method. This happens because quasi-molecular absorptions arise from processes that involve atoms strongly disturbed. In fact, particle interactions, which include variations in both energy and dipole moment of the transition, need be directly considered in the evaluation of such absorption cross-sections (Kowalski 2006b). Therefore, it would be incorrect to use the non-ideal opacity law (13) in the context of far-red wing absorption, since particle perturbations are already explicitly included in expression (10). Of course, HM approach participates in the absorption coefficient (11) as it decides the actual populations of ground-state atoms and perturbers, which take part in the line wing broadening.

4 RESULTS

The properties of the Lyman α broadening can be understood by studying Figs 7 and 8, which show the absorption cross-section of Lyman α line broadened by collisions with H and H_2, respectively, for $T = 6000$ K and perturber density $n_{\rm p} = 10^{20}$ cm^{-3}. These figures also illustrate the photon wavelength for transitions induced in H–H and H–H_2 encounters according to the classical Franck–Condon principle (equation 5).

For H–H collisions, the difference between the upper and lower interatomic potential for $b - a$, $b - i$ and $b - h$ triplet transitions increases (and the wavelength decreases) monotonically with the internuclear separation (bottom panel of Fig. 7). Consequently, their wing spectrum contributions are relatively featureless and extend to long wavelengths from the Lyman α central wavelength at 121.6 nm (top panel of Fig. 7). The potential energy difference for $X - B$, $X - C$ and $X - B'$ transitions does not decrease monotonically with the internuclear separation. Local extrema in the $X - B$, $X - C$ and $X - B'$ energy differences correspond, respectively, to wavelengths $\lambda = 162.3$, 126.8 and 121.8 nm at the red wing, and $\lambda = 83.0$, 82.0 and 73.4 nm at the blue wing. Each extrema can eventually produce a satellite feature in the line wings [a satellite at 162.3 nm was predicted by Sando et al. (1969) and observed in a WD spectrum by Koester et al. (1985)]. These energy extrema yield the classical discontinuities at wavelengths observed in the absorption cross-sections for singlet transitions (Fig. 7). The blue wing due to singlet transitions is caused by the deep well in the ground electronic state of the diatomic molecule. In the far red wing, the $b - a$ transition gives the dominant contribution to the line broadening by H–H collisions. A comparison with the results of Kowalski & Saumon (symbols in the top panel of Fig. 7) shows very good agreement for the dominant absorption at the far red wing.

[4] Notice that the proposal of transitions from bound states to the so-called *dissolved states* considered in Hubeny et al. (1994) is invalid within of HM formalism. For details, see Rohrmann et al. (2002).

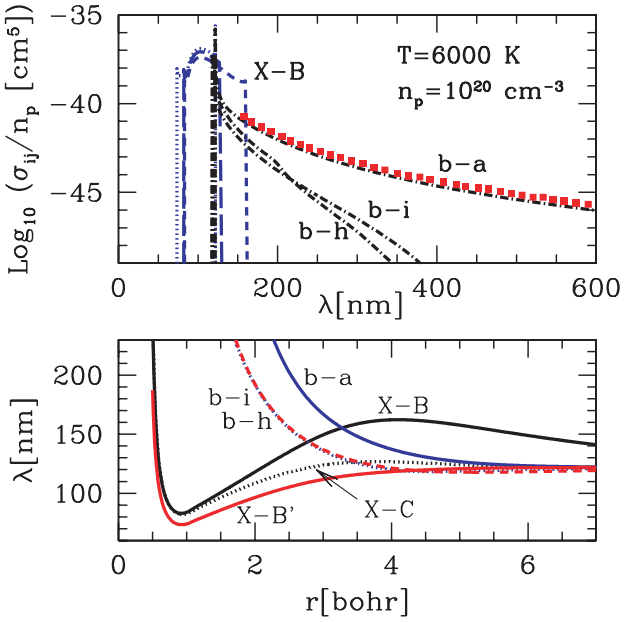

Figure 7. Top panel: cross-sections as given by the quasi-static approach, equation (7), for different transitions in H–H collisions. The dashed line is for $X^1\Sigma_g^+$-$B^1\Sigma_u^+$, long-dashed line is for $X^1\Sigma_g^+$-$C^1\Pi_u^+$ and dotted line is for $X^1\Sigma_g^+$-$B'^1\Sigma_u^+$. Results due to transitions between triplet states are labelled on the plots (dot–dashed lines). The density of perturbers (H atoms) is $n_p = 10^{20}$ cm^{-3} and the gas temperature $T = 6000$ K. Cross-section evaluations of Kowalski (2006a, fig. 49) are shown with symbols. Bottom panel: variation in the wavelength based on the level energy difference (equation 5) of selected transitions for H–H dimers as a function of the internuclear distance. The curves for $b-i$ and $b-h$ transitions are visually identical.

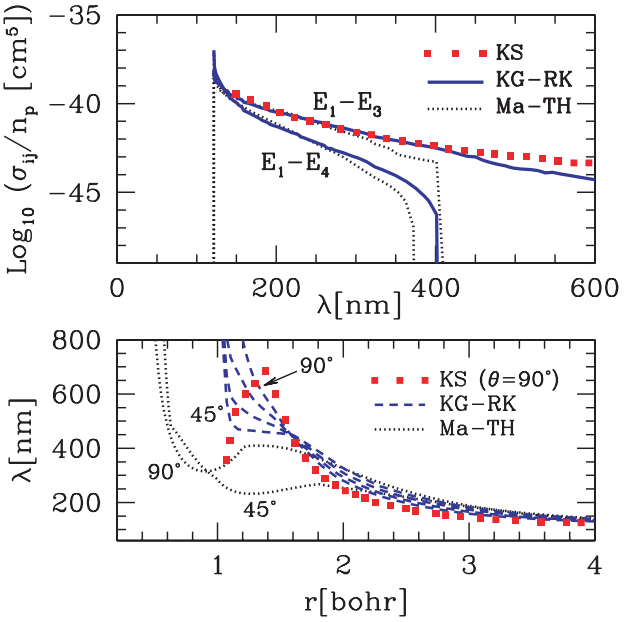

Figure 8. Top panel: cross-sections as given by the quasi-static approach, equation (7), for $E_1 - E_3$ and $E_1 - E_4$ transitions in H_2–H collisions. Notations are given in the text. The density of perturbers (H_2 molecules) is $n_p = 10^{20}$ cm^{-3} and the gas temperature $T = 6000$ K. KS results are taken from Kowalski (2006a, fig. 49). Bottom panel: variation in the wavelength based on the level energy difference (equation 5) of select H_3 transitions as a function of the internuclear distance and for different PES evaluations (indicated on the plot). KG–RK curves correspond to $\theta = 45°$, 60°, 75° and 90°. KS results are based on fig. 48 in Kowalski (2006a).

Allard & Kielkopf (2009) noted in a recent study that simultaneous collisions with more than one perturber give an additional absorption from $X - B$ transitions. Specifically, collisions with multiple atoms yield $X - B$ opacity contributions, which dominate the 180–300 nm region. These multiple collisions could introduce additional absorption features in the UV spectra of DA WDs; however, they have likely no impact over the *UBVRI* photometry of these stars, because the corresponding bandpasses are at longer wavelengths. Furthermore, multiple perturber effects become important at densities as high as 10^{21} particles per cm^3, but the atomic population hardly reaches this value in WD atmospheres due to molecular recombination.

The top panel of Fig. 8 shows the absorption coefficients from $E_1 \rightarrow E_3$ and $E_1 \rightarrow E_4$ transitions in H–H_2 collisions as a function of the wavelength for $T = 6000$ K and molecular density $n_{H_2} = 10^{20}$ cm^{-3}. The variations in the wavelength with the H–H_2 distance are also given in Fig. 8 (bottom panel). The KG–RK label denotes results based on interpolations of PESs calculated by KG and Roach & Kuntz (1986) as described in Section 2.3, while the Ma–TH label corresponds to results obtained from analytical fits of E_1 and E_3 (E_4) PESs due to TH and Ma, respectively.

According to the semiclassical approximation, no broadening of the Lyman α transition due to H_2 molecules will occur for $\lambda < 121.6$ nm (bottom panel in Fig. 8). Cross-sections based on KG–RK energy surfaces (solid lines in the top panel of Fig. 8) show that the far wing broadening by H_2 is dominated by the transition $E_1 - E_3$ and originated from short-range interactions ($r \lesssim 2$ Bohr). The $E_1 - E_4$ transition gives an important contribution in the near wing ($\lambda < 150$ nm) but yields smaller cross-section values than the $E_1 - E_3$ transition to longer wavelengths. As a remarkable feature, the cut-off at $\lambda = 400$ nm in the $E_1 - E_4$ absorption is caused by the reduction in the dipolar moment at short internuclear distances (Fig. 5).

Fig. 8 (bottom panel) shows that the wavelengths derived from KS potentials at $\theta = 90°$ are below the KG–RK values at relatively great distances (1.5–4 Bohr), above those values at intermediate distances (1.3–1.5 Bohr) and finally falls at short distances ($r < 1.3$ Bohr). Such differences are relatively small in H–H_2 separations, where the far wing is formed so that both calculations yield similar cross-sections, as it can be appreciated in Fig. 8 (top panel). Compared with results based on KG–RK energies, KS absorptions increase slightly towards long wavelengths ($\lambda > 450$ nm) likely as a result of the energy discrepancies found between 1.3 and 1.5 Bohr.

Fig. 8 also shows that the opacities calculated with Ma–TH PESs (dotted lines) are similar to other reported results for wavelengths shorter than 250 nm, but then fall sharply at longer wavelengths. Discrepancies are particularly severe for the $E_1 - E_3$ transition in the optical region ($\lambda > 400$ nm). In this figure (bottom panel), one can see that the cross-section at visible wavelengths is governed primarily by the energy difference between the initial and final states in the H_3 transitions at atom–molecule separations smaller than 2 Bohr. At these distances, wavelengths derived from Ma–TH PESs notably differ from KG–RK and KS results. In particular, Ma–TH curves exhibit a local maximum about 400 nm for $\theta = 90°$ (shorter wavelengths for decreasing collision angles). Consequently, opacities based on Ma–TH energies have a dramatic long-wavelength reduction as shown in the top panel of Fig. 8. Further analysis shows that these discrepancies are mainly due to the different behaviours of the PESs used for the Rydberg states.

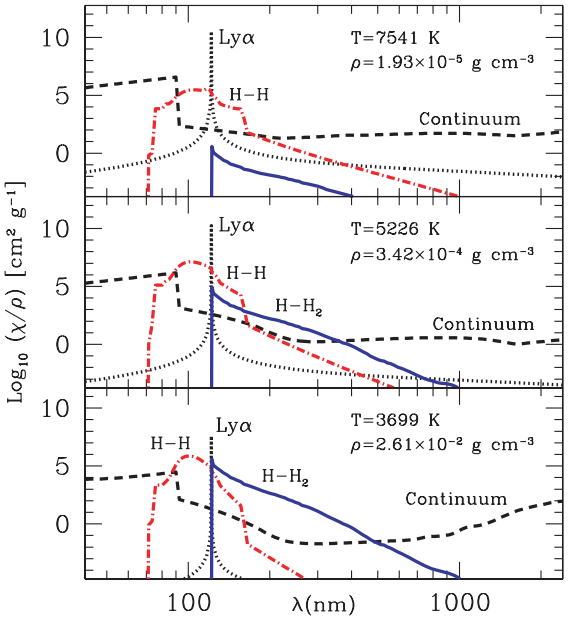

Figure 9. Monochromatic opacity coefficient in the photosphere ($\tau_{\rm Ross} = 1$) of H model atmospheres at $\log g = 8$ and $T_{\rm eff} = 7000$ K (top panel), 5000 K (middle panel) and 3000 K (bottom panel). Shown are the total continuum opacity without Lyman α absorption (dashed lines), the individual contributions to Lyman α wing broadening by H (dot–dashed lines) and H_2 (solid line), and the Stark-broadened Lyman α profile (dotted lines) of Vidal, Cooper & Smith (1973). Temperature and gas density values are indicated on the plot.

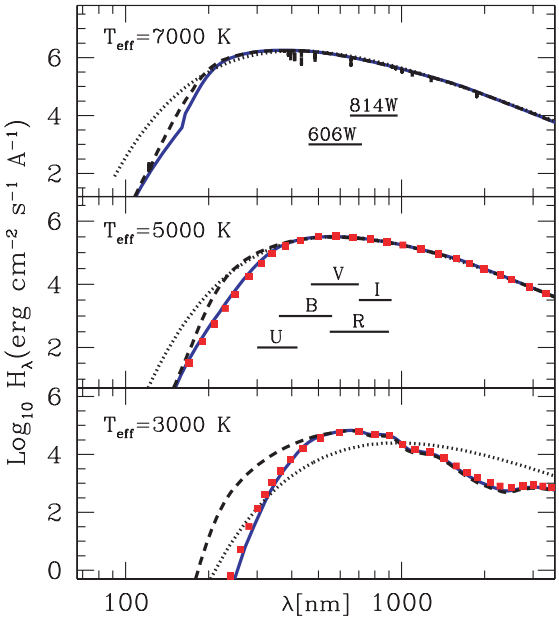

Figure 10. Emergent spectra calculated for hydrogen pure atmosphere models with (solid lines) and without (dashed line) collision broadening of Lyman α at $\log g = 8$ and $T_{\rm eff} = 7000$ K (top panel), 5000 K (middle panel) and 3000 K (bottom panel). The dotted lines represent blackbody spectra at $T = T_{\rm eff}$. For comparison, the synthetic spectra computed by Kowalski (2007) for $T_{\rm eff} = 3000$ and 5000 K are shown with symbols. The short solid lines indicate the location of the transmission functions for the filters *F606W* and *F818W* of the *HST* ACS (Vega-mag system) and those of the *UBVRI* photometry.

Taking into account that absorption cross-section values are very sensitive to small changes in the difference between the PESs of H_3 states, we are inclined to believe that KG and RK evaluations (which give simultaneous evaluations of E_1 and E_3 energies) provide a better internal consistency than the use of TH and Ma analytical fits, which are based on different energy computations for E_1 and E_3 states. A conclusion of our study is that reliable evaluations of H_3 PESs covering a large region of nuclear configurations are needed for a better description of H–H_2 collisions and an accurate evaluation of their influence on Lyman α wing broadening. Results shown henceforth are based on KG–RK energies.

The importance of the collision-induced broadening of the Lyman α line can be appreciated in Fig. 9, which displays the total continuous monochromatic opacity (dashed lines) and the Lyman α wing broadening by H (dot–dashed lines) and H_2 (solid lines) as a function of the wavelength for different physical conditions of a hydrogen gas. These evaluations correspond to the Rosseland optical depth $\tau_{\rm Ross} = 1$ of pure hydrogen model atmospheres at $\log g = 8$ and $T_{\rm eff} = 7000$ K (top panel), 5000 K (middle panel) and 3000 K (bottom panel). For the sake of comparison, we depict the Stark broadening Lyman α profile (Vidal et al. 1973) (dotted lines) that accounts for the main source of broadening in most relatively hot WDs ($T_{\rm eff} > 10\,000$ K). This broadening mechanism, which is due to charged particle interactions, markedly weakens for the low $T_{\rm eff}$ analysed here.

For the highest temperature considered in Fig. 9, $T = 7541$ K, the absorptions originated from singlet transitions in H–H interactions dominate the gas opacity coefficient between 91 nm (the Lyman jump) and 160 nm. The red wing of Lyman α is sensitive to the degree of molecular recombination in the gas, because that determines the relative importance of broadening by atoms and molecules. At temperatures lower than $T \lesssim 5000$ K and densities greater than $\rho \approx 0.0003$ g cm^{-3}, the degree of dissociation has been reduced to 40 per cent and the far red wing exhibits an enhanced contribution due to H–H_2 collisions. Below $T = 4000$ K, the atoms are surrounded mostly by molecules and the broadening by H_2 dominates the total gas opacity from the Lyman α core up to about 500 nm, while H–H absorption remains as the main opacity source at wavelengths bluewards of the Lyman α line. These results based on KG–RK energies are in agreement with those obtained by KS.

Synthetic spectra of DA WD atmospheres with $\log g = 8$ and $T_{\rm eff} = 3000$, 5000 and 7000 K are shown in Fig. 10. The short-wavelength spectrum of the $T_{\rm eff} = 7000$ K model is clearly affected by H_2 quasi-molecular absorption between the Lyman α core and ≈200 nm. The only prominent feature in this spectral region is the little jump at 160 nm originated by the $X^1\Sigma_g^+ - B^1\Sigma_u^+$ transition. At $T_{\rm eff} = 5000$ K, the contribution from H_3 transitions becomes dominant farther away from the line centre as described above and significantly weakens the emergent radiation for $\lambda \lesssim 450$ nm. At the coolest model, $T_{\rm eff} = 3000$ K, the broadening by H_2 results in a Lyman α wing extending far into the optical region (up to ≈500 nm). The computed flux distribution emerges around the minimum in the opacity caused by two collision-induced absorptions, the H_2–H_2 infrared vibrational bands and the Lyman α wing broadening by H–H_2 encounters. A comparison in Fig. 10 of our new synthetic spectra (solid lines) with evaluations from Kowalski (2007) (symbols) for $T_{\rm eff} = 3000$ K and 5000 K shows an excellent agreement.

The collision-induced wing absorption does not significantly affect the structure of cool WD atmospheres, since most of the flux is radiated at longer wavelengths. However, large deviations from the

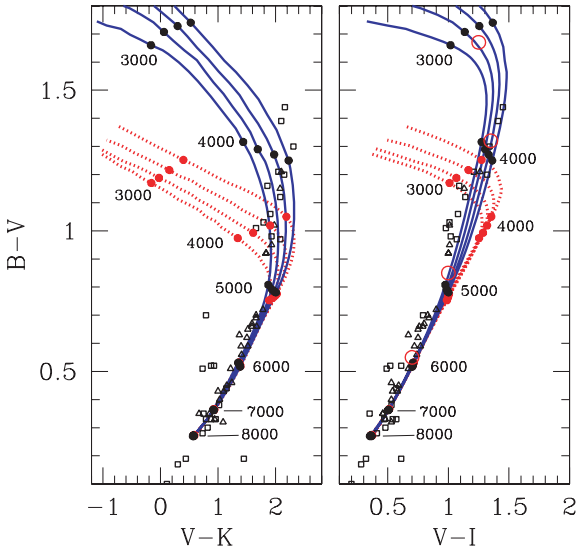

Figure 11. $[(B-V),(V-K)]$ and $[(B-V),(V-I)]$ two-colour diagrams for hydrogen models with $\log g$ values of 7.0, 7.5, 8.0 and 8.5 (from the top to bottom panel). The solid and dotted lines represent models with and without the collision-induced wing of the Lyman α line, respectively. Select $T_{\rm eff}$ values are labelled along the curves. Observations of DA (squares) and non-DA (triangles) WDs are taken from Bergeron et al. (2001). Evaluations from Kowalski & Saumon (2006) at $\log g = 8$ and $T_{\rm eff} = 6000$, 5000, 4000 and 3000 K are shown as the open circles.

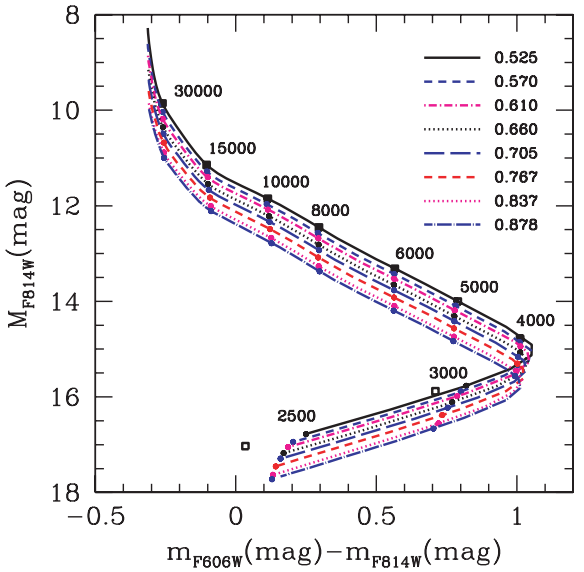

Figure 12. (M_{F814W}, $m_{F606W} - m_{F814W}$) colour–magnitude diagram for WD sequences with masses 0.525, 0.570, 0.610, 0.660, 0.705, 0.767, 0.837 and 0.878 $M_\odot$. Pure hydrogen atmospheres are assumed. Results for selected values of $T_{\rm eff}$ are indicated with the fill circles. The open squares correspond to the situation in which the Lyman α collision broadening is not considered for the 0.525-$M_\odot$ model.

UV and blue colours are predicted with this opacity. In Fig. 11, we show the computed $(B-V, V-K)$ and $(B-V, V-I)$ two-colour diagrams for our new models (solid lines) compared to observations (symbols) and previous model calculations without the Lyman α red wing (dotted lines). These atmosphere model sequences correspond to $\log g = 7$, 7.5, 8 and 8.5 (from the right-hand side to left-hand side). The effects of excluding the new opacity source are clearly visible on the $B-V$ colour, giving rise to an increase of approximately 0.5 mag at the coolest models. This additional opacity does not affect V and redder filters significantly. The comparison with the observed sequence of cool WDs (Bergeron, Leggett & Ruiz 2001) shows that the new models reproduce the observations much better than the old models. In particular, we can see that the colours of the calculated models follow better the tendency of a linear sequence that the observations indicate. On the other hand, the sequence at $\log g = 8$ displayed in the $(B-V, V-I)$ diagram is very close to values obtained by KS at select $T_{\rm eff}$ and for the same surface gravity.

Fig. 12 displays a colour–magnitude diagram using *HST* ACS filters (Vega-mag system) for DA WD cooling sequences of several stellar masses in the range $0.52 < M(M_\odot) < 0.88$. A similar diagram was shown in Kowalski (2007) for $M = 0.5\,M_\odot$. Present calculations are based on a homogeneous set of evolutionary cooling tracks of hydrogen-rich DA WDs (Renedo et al. 2010). These models take into account the most up-to-date physical inputs, including the complete evolutionary history of progenitor stars, element diffusion, chemical stratification, carbon–oxygen phase separation and crystallization processes. Fig. 12 shows that the Lyman α quasi-molecular opacity reduces the shift to the blue due to the H_2 collision-induced infrared absorption in the cool extreme of the sequences. As a result of Lyman α opacity, the M_{F814W} magnitude and the $m_{F606W} - m_{F814W}$ colour turn out to be 100–200 K cooler, thus implying a larger age for a WD of a given stellar mass (see also Kowalski 2007).

5 CONCLUSIONS

KS identified the missing absorption in the blue and UV radiation of cool WDs due to Lyman α broadening by H–H_2 collisions. Here, we present independent calculations for the collision-induced broadening of the Lyman α line in dense gases typical of cool WD atmospheres. Our results largely agree with those of KS. Quasi-molecular lines in these atmospheres arise from radiative collisions of excited atomic hydrogen with unexcited neutral molecules H_2 or atoms H. As given in KS, present line opacity evaluations are based on the quasi-static approach, which relies on the nearest perturber approximation and the Franck–Condon principle. Line-broadening processes are therefore described in terms of independent absorptions occurring during collisions between a hydrogen atom and a perturber, either another H atom or a H_2 molecule.

We revisit the properties of DA stars in the range $8000 > T_{\rm eff} > 2500$ K by analysing the synthetic spectra with our improved models. The broad-band colours located in the UV and blue spectral regions are shown to differ substantially from those published in previous studies, which did not include collision-induced Lyman α wing absorptions. Full tables containing both cross-sections of collisionally broadened Lyman α wings and WD colours are available at http://www.fcaglp.unlp.edu.ar/evolgroup or upon request to the authous at their e-mail addresses.

This study points out that a detailed knowledge of the simplest polyatomic molecule, H_3, is of fundamental importance for a precise understanding of Lyman α opacity processes in cool WDs. Accurate PESs are required for their excited electronic states in order to precisely account for the effects of H–H_2 collisions on the UV and visible spectra of these stars.

ACKNOWLEDGMENTS

We thank Piotr Kowalski for providing us with his computer data for comparisons. RDR acknowledges Boothroyd for valuable comments. Part of this work was supported by the CONICET project number PIP 112-200801-01474 and PIP 112-200801-00940, and by AGENCIA through the Programa de Modernización Tecnológica BID 1728/OC-AR.

REFERENCES

Allard N. F., Kielkopf J. F., 1982, Rev. Mod. Phys., 54, 1103
Allard N. F., Kielkopf J. F., 2009, A&A, 493, 1155
Allard N. F., Royer A., Kielkopf J. F., Feautrier N., 1999, Phys. Rev. A, 60, 1021
Allard N. F., Hébrard G., Dupuis J., Chayer P., Kruk J. W., Kielkopf J. F., Hubeny I., 2004, ApJ, 601, L183
Althaus L. G., Córsico A. H., Isern J., García-Berro E., 2010, A&AR, 18, 471
Bates D. R., 1951, MNRAS, 111, 303
Bergeron P., Leggett S. K., Ruiz M. T., 1997, ApJS, 108, 339
Bergeron P., Leggett S. K., Ruiz M. T., 2001, ApJS, 133, 413
Bethe H. A., Salpeter E. E., 1957, Quantum Mechanics of One- and Two-Electron Atoms. Academic Press Inc., Berlin
Boothroyd A. I., Keogh W. J., Martin P. G., Peterson M. R., 1991, J. Chem. Phys., 95, 4343
Boothroyd A. I., Keogh W. J., Martin P. G., Peterson M. R., 1996, J. Chem. Phys., 104, 7139
Borysow A., Jorgensen U. G., Fu Y., 2001, JQSRT, 68, 235
Chen S. Y., Takeo M., 1957, Rev. Mod. Phys., 29, 20
Doyle R. O., 1968, ApJ, 153, 987
Dressler K., Wolniewicz L., 1985, J. Chem. Phys., 82, 4720
Eisenstein D. J. et al., 2006, ApJS, 167, 40
Field G. B., Sommerville W. B., Dressler K., 1966, ARA&A, 4, 207
Ford A. L., Browne J. C., Shipsey E. J., DeVries P., 1975, J. Chem. Phys., 63, 362
Gallager A., Holstein T., 1977, Phys. Rev. A, 16, 2413
Gustafsson M., Frommhold L., 2003, A&A, 400, 1161
Hansen B., 1998, Nat, 394, 860
Hirschfelder J. O., Curtiss C. F., Bird R. B., 1954, Molecular Theory of Gases and Liquids, Wiley, New York
Hubeny I., Hummer D. G., Lanz T., 1994, A&A, 282, 151
Hummer D. G., Mihalas D., 1988, ApJ, 331, 794 (HM)
Jablonski A., 1945, Phys. Rev., 68, 78
Koester D., Wolff B., 2000, A&A, 357, 587
Koester D., Weidemann V., Zeidler -K. T. E.-M., Vauclair G., 1985, A&A, 142, L5
Kolos W., Wolniewicz L., 1965, J. Chem. Phys., 43, 2429
Kowalski W., 2006a, PhD thesis, Univ. Vanderbilt
Kowalski W., 2006b, ApJ, 651, 1120
Kowalski W., 2007, A&A, 474, 491
Kowalski W., Saumon D., 2006, ApJ, 651, L137 (KS)
Kulander K. C., Guest M. F., 1979, J. Phys. B, 12, L501 (KG)
Liu B., 1973, J. Chem. Phys., 58, 1925
Margeneau H., Lewis M., 1959, Rev. Mod. Phys., 31, 569
Mayne H. R., Polanyi J. C., Sathyamurthy N., Raynor S., 1984, J. Phys. Chem., 88, 4064 (Ma)
Mielke S. L., Garret B. C., Peterson K. A., 2002, J. Chem. Phys., 116, 4142
Mihalas D., 1978, Stellar Atmospheres, 2nd edn. Freeman, San Francisco
Nelan E. P., Wegner G., 1985, ApJ, 289, L31
Peng Z., Kristyan S., Kuppermann A., 1995, Phys. Rev. A, 52, 1005
Petsalakis I., Theodorakopoulos J., Wright J. S., 1988, J. Chem. Phys., 89, 6850
Raynor S., Herschbach D. R., 1982, J. Chem. Phys., 86, 1214
Renedo I., Althaus L. G., Miller Bertolami M. M., Romero A. D., Córsico A. H., Rohrmann R. D., García-Berro E., 2010, ApJ, 717, 183
Roach A. C., Kuntz P. J., 1986, J. Chem. Phys., 84, 822 (RK)
Rohrmann R. D., 2001, MNRAS, 323, 699
Rohrmann R. D., Zorec J., 2006, Phys. Rev. E, 74, 041120
Rohrmann R. D., Serenelli A. M., Althaus L. G., Benvenuto O. G., 2002, MNRAS, 335, 499
Salaris M., García-Berro E., Hernanz M., Isern J., Saumon D., 2000, ApJ, 544, 1036
Sando K., Wormhoudt J. C., 1973, Phys. Rev. A, 7, 1889
Sando K., Doyle R. O., Dalgarno A., 1969, ApJ, 157, L143
Serenelli A. M., Rohrmann R. D., Althaus L. G., Benvenuto O. G., 2001, MNRAS, 325, 607
Siegbahn P., Liu B., 1978, J. Chem. Phys., 68, 2457
Staszewska G., Wolniewicz L., 1999, J. Mol. Spectr., 198, 416
Stewart J. C., Peek J. M., Cooper J., 1973, ApJ, 179, 983
Truhlar D. G., Horowitz C. J., 1978, J. Chem. Phys., 68, 2466 (TH)
Truhlar D. G., Horowitz C. J., 1979, J. Chem. Phys., 71, 1514 (TH)
Vidal C. R., Cooper J., Smith E. W., 1973, ApJS, 25, 37
Wiese W. L., Kelleher D. E., Paquette D. R., 1972, Phys. Rev. A, 6, 1132
Wolff B., Koester D., Liebert J., 2002, A&A, 385, 995
Wolniewicz L., Dressler K., 1988, J. Chem. Phys., 88, 3861

This paper has been typeset from a TEX/LATEX file prepared by the author.